2009

Diagnostics for Ultracold Plasma Experiments

Lauren Rand
Colby College

Diagnostics for Ultracold Plasma Experiments

Lauren Rand

Honors Thesis

Department of Physics and Astronomy

Colby College

Waterville, Maine

Advisor: Professor Duncan A. Tate

May 2009

Abstract

The goal of this experiment was to observe the effects of variations of experimental conditions on the ultracold plasma that formed as a result. The wavelength and power of the ionizing laser were varied to change the electron temperature and plasma density. The delay between the ionizing laser and the field ionization pulse was changed as well. In each case, plasma evolution and the resulting distribution of Rydberg states were observed. It was found that both electron temperature and plasma density directly affected the plasma lifetimes. However, neither electron temperature nor plasma density nor delay length had an effect on the distribution of the Rydberg states. Future experiments are planned to observe the effects of a prematurely quenched plasma on the distribution of Rydberg states formed.

Acknowledgements

I would like to start by thanking Prof. Tate for all of his help. He spent a lot of time with me in the lab, helping me getting everything to work and answering what must have seemed like an endless stream of questions. He encouraged me to figure things out on my own, but gave me guidance when I needed it. I really appreciate his generosity and patience, and I have learned a lot.

I would also like to thank Profs. Bluhm, Conover, Long, Campbell and Lisa Lessard. Throughout the last four years, they have taught me more than just physics. I've learned an entirely new way of thinking about the world around me. I'd especially like to thank Prof. Bluhm for helping me build a homemade cloud chamber my first year, which caused me to fall in love with experimental physics.

I have a huge amount of gratitude toward my family. The telescope that my parents got me changed my life, and they have always been supportive of my passions (except that one time that I tried to wake them up at 3:00 am to see a UFO). I'd also like to acknowledge my brothers, Devin and Cory, who are generous enough to occasionally ask me a question about physics and then listen to me talk for an hour.

Lastly, I'd like to apologize to my grandmother for choosing to pursue a career in the sciences rather than going to medical school. Sorry Nana.

Table of Contents

List of Figures

Chapter 1: Introduction

The purpose of the experiments described in this thesis was to perform various diagnostic measurements on an ultracold plasma. The defining characteristic of a plasma is its free electrons. Instead of being bound to individual atoms, the plasma electrons are able to move around and are "shared" by all the ions. Plasma is often considered to be a fourth state of matter, due to the physical and chemical properties that set it apart from solids, liquids, and gases. Because of the frequency with which it occurs in non-terrestrial environments, plasma is thought to be the most common state of matter in the universe.

Plasma research can be traced back as far as the early 1900s to the Nobel prize-winning chemist Irving Langmuir. While writing his doctoral thesis about improving light bulbs, Langmuir started to look at the ions emitted from the heated filament, calling them "plasma". He later made the important distinction between electron temperature and plasma temperature, and created an instrument, the Langmuir probe, to measure the temperature of the plasma electrons.

Today, plasma research has evolved to include many different sub-categories, one of which is ultracold plasmas (UCPs). In 1999, *T.C. Killian et al.,* first reported the creation of UCPs through laser photoionization [1]. This was followed in 2000 by a publication by *S. Kulin et al.,* which correlated the resonant frequency of a plasma to its density, which produced a much

more detailed picture of UCP evolution [2]. In 2004, *J.L. Roberts et al.,* proved that the electrons in the UCPs produced were strongly coupled [3]. UCPs are defined by two unique characteristics. One is the plasma temperature. Ion temperatures in UCPs are in the range of 10 μK to 1 mK. The other defining attribute is that the Coulomb force experienced by the ions and electrons within the plasma dominates their motion. Because their temperatures are so low, the electron and ionic kinetic energies are very small. As a result, the Coulomb interactions between the electrons and ions are stronger than the inherent tendency to fly apart caused by kinetic energy. A UCP is therefore considered to be a "strongly coupled" plasma, whereas other common sources of plasma are not. Interest in UCPs has increased recently due to changes in behavior that occur within the plasma as it approaches the ultracold temperatures. A behavior that is investigated in this thesis is the recombination that can occur, in which an electron and an ion reunite to create an atom. In a UCP, the dominant method by which this phenomenon occurs is known as three-body recombination, wherein the electron and the ion recombine and a second electron is involved to conserve momentum and energy. In no other type of plasma is this process so common [4]. In 2007, *R.S. Fletcher, X.L. Zhang, and S.L. Rolston* correlated the recombination rate to electron temperature [5].

UCPs are generally created by laser excitation of atoms in a vacuum chamber. The experiments take place in a carefully controlled environment, where the plasma conditions can be chosen and varied. At the Colby College laboratory, rubidium atoms are cooled in a magneto-optical trap (MOT) and then excited to form the UCP. Rubidium is chosen because of its single valence electron. The electron is sufficiently loosely bound that it is possible to ionize the atom with a carefully tuned, low-powered laser. In addition, the vapor pressure of

rubidium is high enough that it can be vaporized by low temperatures. Natural rubidium occurs primarily in two isotopes; ^{87}Rb and ^{85}Rb. In the Colby lab, ^{85}Rb is used because it is more common than ^{87}Rb, and this makes the MOT operation more reliable. However, simple adjustments to the laser frequencies would allow the use of ^{87}Rb.

Chapter 2: Apparatus

2.1 Ultracold Plasma Formation

Ultracold plasmas are formed by photoionizing cold atoms in a magneto-optical trap. In our apparatus ^{85}Rb atoms were cooled using diode lasers and trapped using a magnetic field.

2.2 Chamber

All ultracold plasma experiments must take place within a high vacuum, less than 10^{-9} torr. This is required for plasma evolution experiments, and allows the MOT to operate and trap an adequate number of atoms. A cylindrical steel chamber in conjunction with a high vacuum pump provides such an environment. An ion pump is used, which allows the achievement of pressures as low as $1x10^{-10}$ torr. The chamber itself is fitted with six windows that allow the passage of laser beams in and out along the three spatial axes. In addition to the windows, there are several feed-throughs that allow the application of electric fields within the chamber. The height of the chamber is 300 mm and it has a diameter of 150 mm. Two wire coils are arranged around the chamber in an anti-Helmholtz configuration to provide a spatially varying magnetic field, as can be seen in Fig. 1. The application of a voltage to two wire meshes

arranged around the center of the chamber causes the production of an electric field around plasma.

Figure 1: A picture of the vacuum chamber in the Colby College laboratory. One of the windows and parts of the coils in the anti-Helmholtz configuration may be seen.

Connected to the chamber is a rubidium "finger" that can be opened to the vacuum chamber. The rubidium finger is filled with a large pellet of rubidium. To facilitate its release into the main chamber, the finger is heated to create rubidium vapor. It is this rubidium vapor that is laser and magnetically cooled, ionized, trapped, and eventually formed into plasma.

2.3 External Cavity Diode Lasers

Two external cavity diode lasers (ECDLs) are used in the formation and cooling of the cold atom sample, the trap laser and the repump laser. Each of these lasers has two main components; an oscillator ECDL, and a non-cavity diode laser amplifier. For both lasers,

immediately after exiting the ECDL housing, the beam is sent through an optical isolator that prevents the beam from reflecting back into the ECDL mechanism and detuning the laser [6].

The trap laser configuration will be discussed, but it is important to note that the repump laser configuration is very similar. After passing through the isolator, the beam from the trap laser oscillator is split and one part is sent through an 8 cm long glass rubidium cell. A photodiode on the other side measures the intensity of the transmitted beam, and thus, how much of the beam was absorbed by the rubidium. If the laser is tuned to a frequency that corresponds to a transition, some of the light goes toward exciting the atoms and thus does not come out the other end, so the intensity is lower. This tuning process occurs assuming that there is no Doppler shift present. This allows us to tune the beam to a specific transition. The beam is tuned to a frequency approximately 45 MHz below the frequency of the cooling transition (^{85}Rb $5s_{1/2}$ F=3 to $5p_{3/2}$ F=4). That transition involves a very small change in intensity of the beam, so it is very difficult to effectively lock the laser on to it. Instead, we pick larger crossover transition nearby that is a known frequency interval away from the desired one that is easy to lock on. The beam that does not go to the locking mechanism passes through an acousto-optic modulator which up-shifts the frequency by 45 MHz to tune it to the correct cooling frequency.

From the acousto-optic modulator, the beam goes to an injection-locked diode laser amplifier, which emits a more powerful laser at the same wavelength as the seed beam. The amplified beam passes through a second isolator before being directed toward the MOT chamber. In the operation of the system, the trap oscillator beam is tuned to the correct

frequency, and then the trap amplifier is injection-locked to it by tuning its current. Only after the amplifier is functioning is the oscillator beam locked at its correct frequency. The full schematic can be seen in Fig. 2.

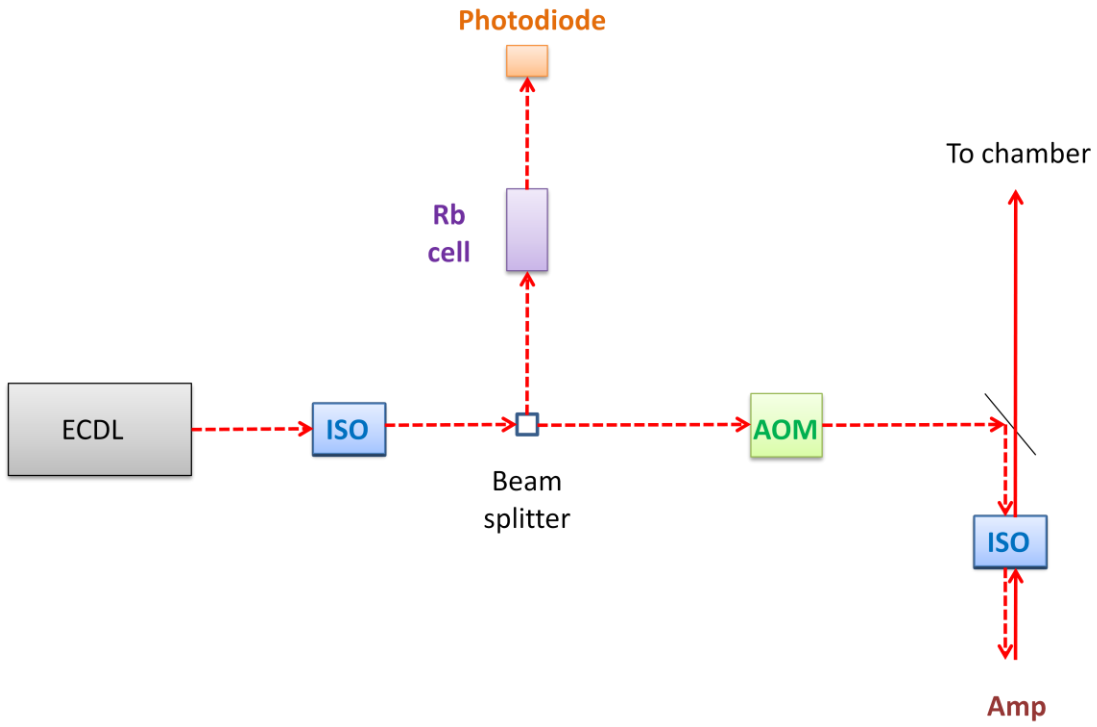

Figure 2: A schematic of the trap laser system. The oscillator ECDL beam passes through an optical isolator (ISO) before being split. Part of the beam is sent to the Rb cell to be tuned, while the other part is sent through an acousto-optic modulator (AOM), through an isolator (ISO) and then to an amplifier.

The beam is split by prisms into three components that are directed along the three orthogonal spatial axes. Before entering the chamber, the beam is sent through a quarter wave plate which gives it a circular polarization. The beam passes through a window, into the chamber, and exits through another window. The exiting beam is reflected by a mirror back into the chamber along the same axis. However, before reentering the chamber, the beam is sent through a second quarter wave plate which gives it a polarization of the opposite circularity than that with which it started, as seen in Fig. 3.

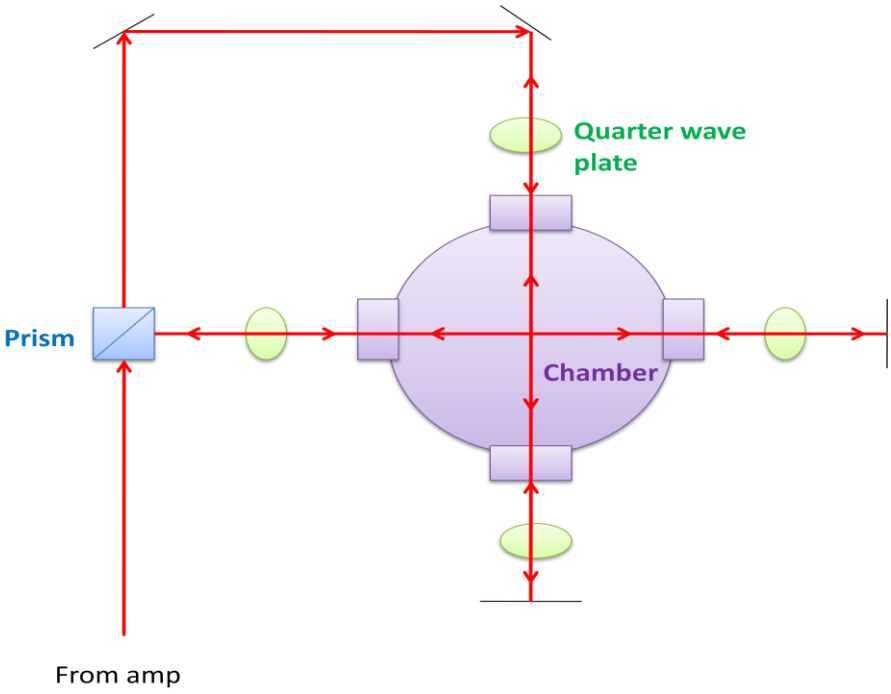

Figure 3: A schematic of the optical system around the vacuum chamber. The beam is split and directed along the three spatial axes, and then sent through quarter wave plates before entering the chamber. Upon exiting the chamber, the beams are reflected back in along the same direction after passing through another set of quarter wave plates. This diagram only shows the system in the x-y plane, but there is also a beam directed along the z-axis.

2.4 Photoionization Laser

A pulsed, dye-amplified laser is responsible for the actual formation of the plasma. The setup is based on a commercially available Littman ECDL (Sacher Lasertechnik TEC-520-0960-100) with a high degree of stability. The Littman ECDL is set to a wavelength of approximately 960 nm, although it may be tuned to meet the requirements of the experiment [7, 8].

The amplification comes from a neodymium-doped yttrium aluminum garnet (Nd: YAG) laser. The Nd: YAG laser is pulsed at 20 Hz. A population inversion in the garnet is allowed to build up, at which point a light ray is then allowed to go through and set off the lasing process.

This depletes the inversion buildup, and the light ray is discontinued after 10 ns to give the garnet the opportunity to once again achieve a population inversion. The result is an extremely powerful, pulsed laser emitting a beam with a wavelength of 1064 nm. This can be converted to 532 nm (the second harmonic) and 355 nm (the third harmonic) using nonlinear crystals. The 532 nm Nd: YAG laser beam is split and directed at three dye cells filled with dissolved LDS 925 dye. This has the effect of exciting the dye molecules, which creates a population inversion.

Light from the Littman ECDL is sent through all three dye cells in series. As it goes through, the excited molecules in the cells are stimulated to decay, emitting photons with the same wavelength as the diode laser passing through. This has the effect of amplifying the Littman ECDL to an average power of several milliwatts, which pulses at 20 Hz with 300 μJ of energy per pulse. From the dye cells, the amplified beam is frequency doubled by a potassium niobate crystal to approximately 480 nm, focused, and directed into the MOT chamber. When the wavelength of the Littman ECDL is changed, the wavelength of the photoionization laser, which is measured by a wavemeter, changes as well. The wavelength of the photoionization laser controls the temperature of the electrons, so simple adjustments to the Littman ECDL result in changes in the plasma electron temperature. The schematic of the photoionization laser system can be seen in Fig. 4.

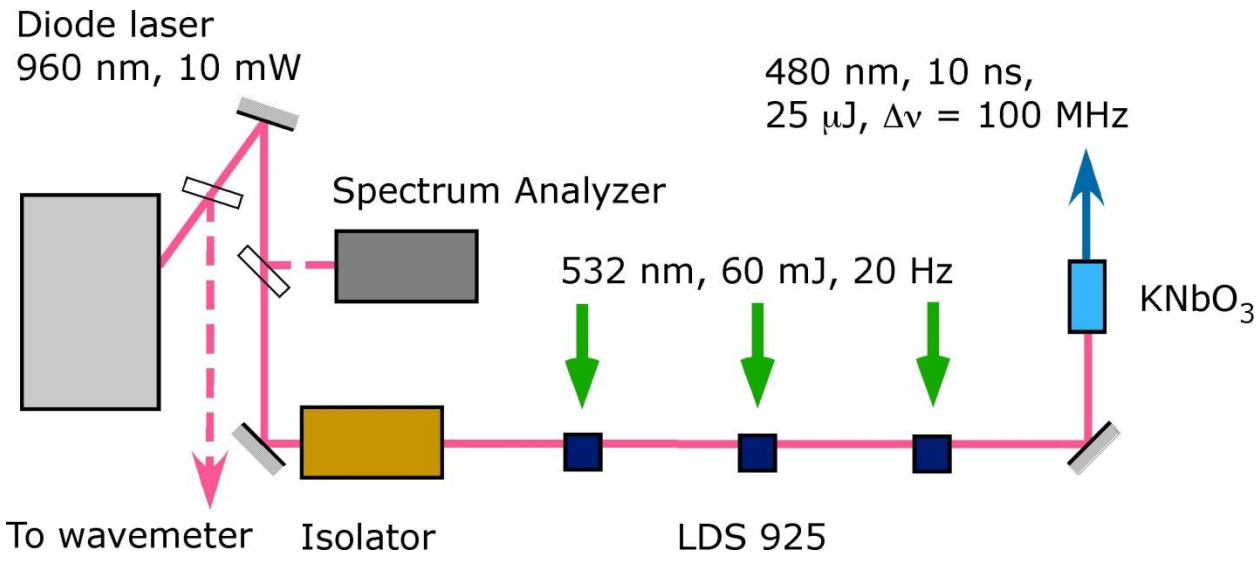

Figure 4: A schematic of the photoionization laser apparatus. A Littman ECDL laser is sent through three blue dye cells filled with LDS 925. The dye cell atoms are excited by a green Nd:YAG laser. When the atoms decay, they amplify the Littman ECDL beam, which is then frequency doubled by a $KNbO_3$ crystal and sent toward the chamber.

Chapter Three: Experiment

3.1 Laser Cooling/Optical Molasses

Low temperatures are vital in the successful formation of an ultracold plasma. A system of lasers and a magnetic field is used to create "optical molasses", which cools the rubidium atoms to temperatures low enough for a plasma to be created when the atoms are photoionized.

The trap laser is responsible for the primary cooling process. It simply works to slow the rubidium atoms' velocities, thus decreasing their kinetic energies and their temperatures. To do this, a photon from the laser transfers momentum to an atom moving in the opposite direction and slows its motion. To absorb the photon's momentum, an electron in the atom must undergo a transition to an excited state. When the electron naturally decays, the atom emits a photon in a random direction. Over a large group of atoms, the momentum vectors created by these emissions cancel one another out and the process does not have an overall effect. As a result, the only momentum change is due to the initial photon absorption from the laser.

The excitation of the electron in rubidium caused by the laser photon at 780 nm is from the $5s_{1/2}$ state to the $5p_{3/2}$ state. Once the electron decays back to its initial state, it may be excited again. It takes many cycles of this process to sufficiently cool the rubidium. However, a

problem arises once hyperfine states are taken into consideration. Ideally, the electron would be excited from the $5s_{1/2}$ F=3 state to the $5p_{3/2}$ F'=4 state. Then the electron would naturally decay back to where it started. But in approximately one in a thousand absorption cycles, the atom is instead excited to the F'=3 state. From this state, there are two allowable decays. The electron can either return to the F=3 state or it can decay to the $5s_{1/2}$ F=2 state. If this latter decay occurs, that atom is in what is known as a "dark state". It is named thusly because it can no longer be excited by the trap laser. As a result, it cannot be further cooled [9].

The repump laser is used to remove these atoms from the dark state. The laser excites the atom from the F=2 state back up to the $5p_{3/2}$ F'=3 state. As a result, the atom has the additional chance to decay back to the F=3 state and reenter the trap laser cooling cycle [1]. A diagram of the allowed excitations and decays and the functions of the trap and repump lasers may be found in Fig. 5.

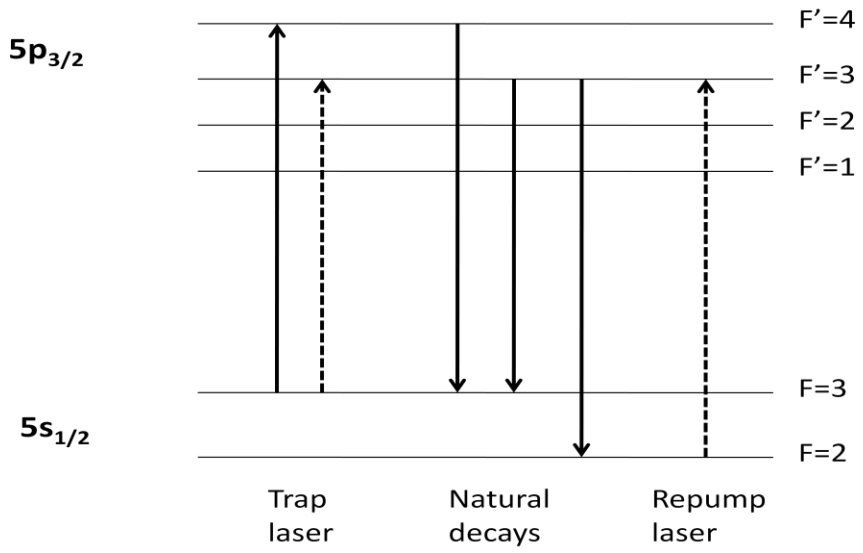

Figure 5: A schematic of the allowed excitations and decays of the rubidium atom. Included are the hyperfine energy states. The F=3 to F'=3 absorption can occur due to the non-zero energy width of the $5p_{3/2}$ hyperfine states.

The trap laser is tuned 10 MHz below the frequency of the $5s_{1/2}$ F=3 to the $5p_{3/2}$ F'=4 transition. This is due to the need to Doppler shift the frequency of the trap laser into resonance for rubidium atoms with velocities opposite to the laser direction. The higher the velocity of the receiving atom, the higher the perceived frequency of the trap laser. As a result, a laser frequency decreased by 10 MHz will target atoms moving in the opposite direction to the laser propagation direction for cooling.

The magnitude of the Doppler shift is dependent on the atomic velocity. To take advantage of this, a magnetic field is applied. The field is applied in a specific configuration that is zero at the center of the chamber, and increases proportionately with the distance away from the center along all three spatial axes. The application of a magnetic field to an atom causes a phenomenon known as the Zeeman Effect. Although the system in the Colby laboratory is significantly more complex, a simple model may be used to discuss the basic events that occur. Assume that the desired cooling transition is from the F=0 hyperfine state to the F'=1 state. The magnetic field removes the degeneracy of the atom's energy levels, causing the three z-components of the F'=1 state's angular momentum, the m_F's, to split into three distinct energy states as shown in Fig. 6. The energy difference between these levels is proportional to the strength of the applied field. The trap laser is tuned to 10 MHz below the F= 0, m_F=0 to the F'=1, m_F=0 transition. The frequency of the trap laser and the slope of the increasing magnetic field are chosen very carefully so that they work together to continuously cool an atom. Consider an atom initially on the right side of the z>0 region, which has a velocity in the –z direction. This atom can absorb a right-handed polarized (σ+) photon (Δm_F=+1) propagating in the +z direction since its velocity will Doppler shift the laser frequency into

resonance in the atom's rest frame. After a few such absorption and emission processes, the atom will still be in the z>0 region, but closer to z=0, and moving more slowly. Consequently, it will see the σ+ photons upshifted by a smaller frequency, but it will still absorb them because the m_F=+1 state is now lower in energy due to the changing magnetic field's Zeeman energy shift [1, 9].

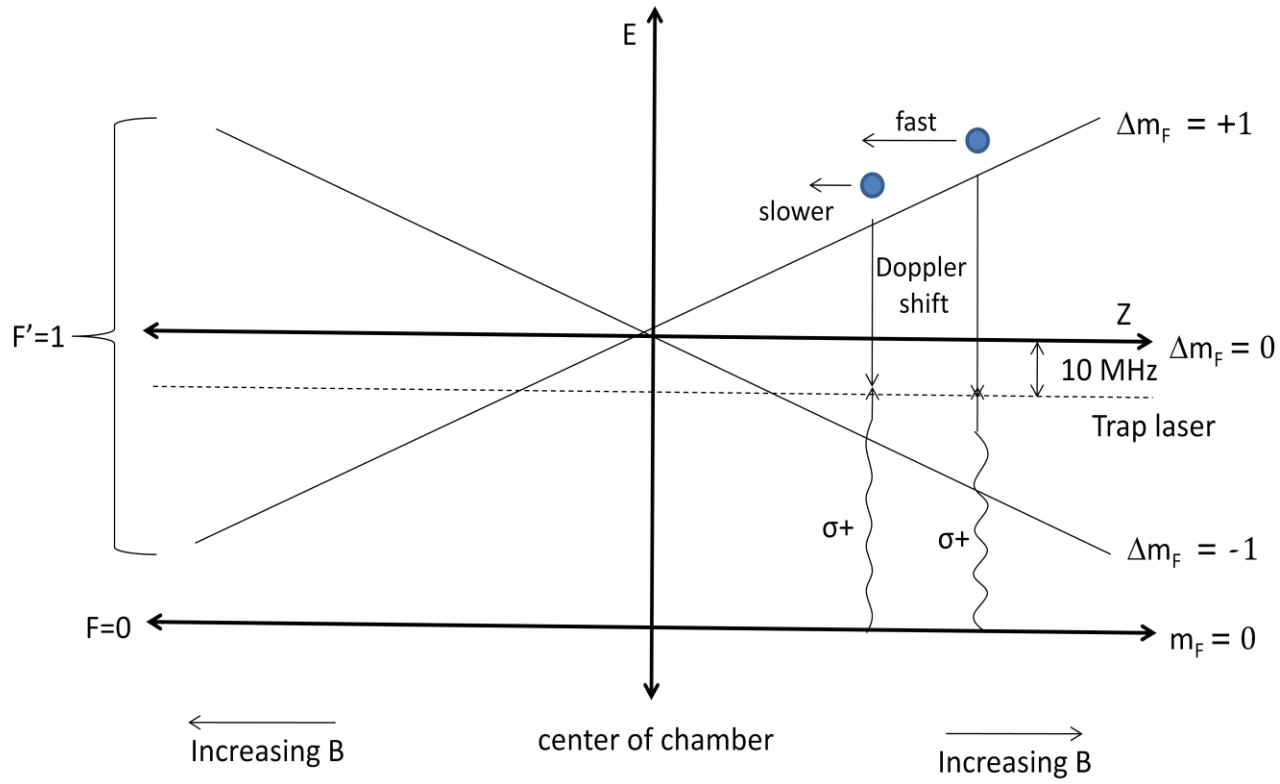

Figure 6: A schematic of the energy level separations created by the spatially variable magnetic field. Included are the tuned trap laser and the amounts of Doppler shift required to alter the beam to the correct frequency.

Circular polarizers are used to give the trap laser a defined polarization. Atoms undergoing a Δm_F=+1 transition are only responsive to beams with a σ+ polarization. Alternatively, the Δm_F=-1 atoms are only excited by the left-handed (σ-) polarized beams. Thus, there is no concern that a laser beam going in the opposing direction will speed up the atoms

and counteract the cooling beam. The atoms are quite literally blind to the beam going in the wrong direction [10].

3.2 Plasma Formation and Evolution

While the trap and repump lasers are working to cool the atoms, the photoionization laser is responsible for photoionizing them to create the plasma. The photoionization laser is used to impart enough energy to the cooled rubidium atoms to fully ionize them and create a mixture of ions and free electrons (plasma). It is assumed that any energy transferred to the atoms in excess of the amount needed for ionization becomes the kinetic energy of the freed electrons.

As soon as the photoionization laser is pulsed and the plasma is created, a small number of electrons escape and are detected. The electrons that escape are from the outer edges of the plasma cloud, where the electron kinetic energy is able to overcome the binding Coulomb forces due to the positive ions (see Fig. 7).

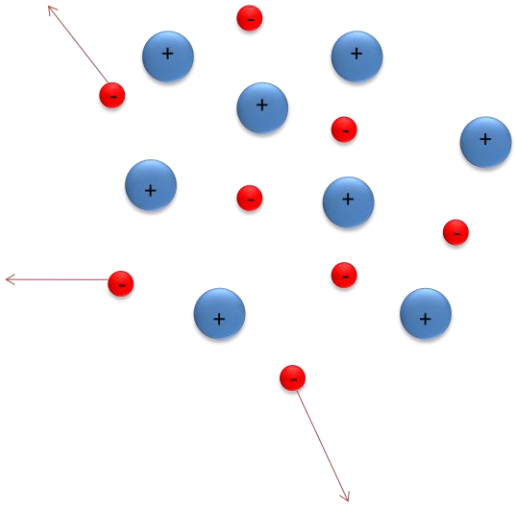

Figure 7: A schematic of the plasma shortly after formation. Outer electrons are able to overcome the potential well and escape, and are then detected.

Once this initial group of electrons leaves the plasma, the rest are more tightly bound by the now overall positive charge of the plasma cloud. The plasma starts expanding due to the repulsive Coulomb forces between the ions. This process occurs slowly due to the large ion masses and low initial velocities (see Fig. 8).

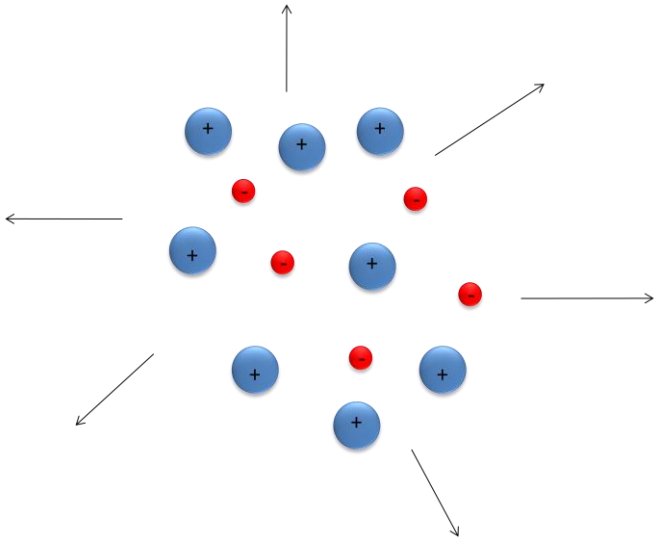

Figure 8: A schematic of the plasma after the initial electrons escape. An overall positive charge causes the ions to repel one another and slowly begin to move apart.

As the plasma expands, electrons located on the boundary soon have enough kinetic energy to escape the potential well created by the attraction to the ions. This causes the plasma cloud to gain an even larger overall positive charge. The cloud continues to expand, the potential well depth for the electrons decreases, and increasing numbers of electrons are able to escape the potential well [2] (see Fig. 9).

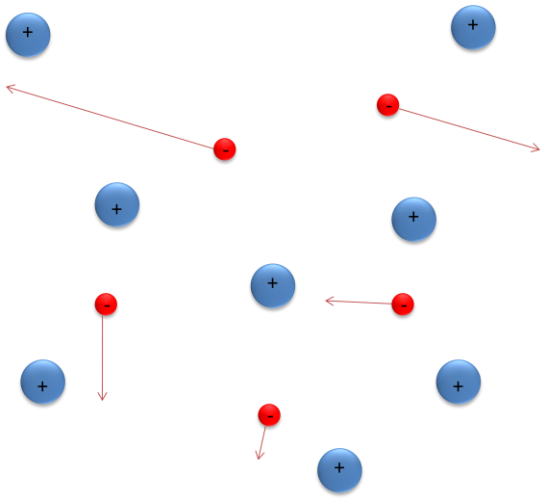

Figure 9: A schematic of the expanding plasma. Electrons begin to escape, leaving the plasma with an even greater positive charge which increases the rate of expansion and allows more electrons to escape.

After a time interval of 10 to 200 μs, the plasma dissipates. The ion cloud has expanded so far that its positive charge can no longer trap electrons, and the ions accelerate apart. The exact amount of time needed for this process is dependent on the initial conditions, at the Colby lab the plasma generally lasts for approximately 60 μs. All the electrons escape and the ions repel one another and dissipate.

3.3 Rydberg formation and detection

During the plasma evolution, it is possible for an electron and ion to recombine and once more become an atom. One of the unique features of ultracold plasmas is the dominant process by which this happens, known as three-body recombination. This process involves two electrons and an ion in a collision. One of the electrons is captured by the ion, and the second electron is used to conserve momentum and energy. Before the collision, the energy of the system is greater than zero. However, after the recombination, the binding energy of the neutral atom formed by one of the electrons and the ion is less than zero. The energy lost in the recombination of the electron and the ion is carried off by the second electron [4].

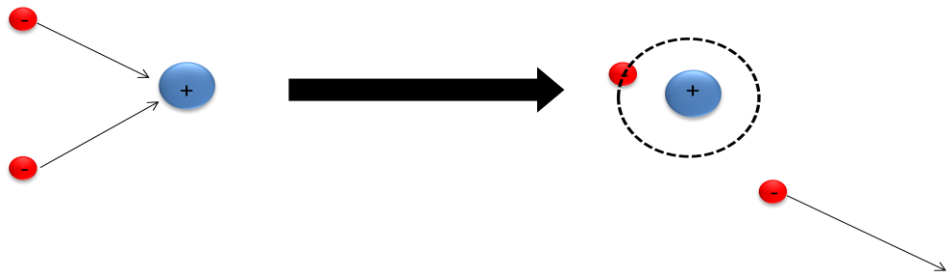

Figure 10: A schematic of three-body recombination. The process involves two electrons and an ion. One of the electrons recombines with the ion, while the other electron is present to conserve momentum and energy.

The atom formed by the recombination process is known as a Rydberg atom. The defining characteristic of a Rydberg atom is the extraordinarily high orbital of the valence electron. The Rydberg atoms created by recombination in the Colby laboratory were found to have an average principle quantum number of n=43. The higher the orbital number, the more loosely bound the electron. As a result, Ryberg atoms may be ionized by exposure to an electric field.

To detect the Rydberg atoms left after the expiration of the plasma, an increasing electric field known as a field ionization pulse is applied. When the field becomes strong enough to ionize the atom, the electron is accelerated by the pulse and may be detected using a microchannel plate detector (MCP). The lower the n state of the Rydberg atom, the larger the field at which the Rydberg atom is ionized. During the 1-2 μs it takes the field ionization pulse to ramp up and reach its maximum voltage, higher n states are ionized first, followed by lower n states. The time of flight of the electrons from the plasma to the microchannel plate detector is negligible, so the electron signal from the field ionization pulse arrives in the order of the Rydberg states energy, with the highest states being "seen" earlier. It is possible to calculate the approximate principle quantum number of the Rydberg from the strength of the field needed to ionize it, according to the equation

$$E = \frac{1}{16n^4} * 5.14\text{x}10^9 \text{ V/cm}$$

where *E* is the adiabatic field ionization threshold, *n* is the principle quantum number, and $5.14\text{x}10^9$ V/cm is the atomic unit for the electric field.

Fig. 11 demonstrates the complete evolution cycle of an ultracold plasma. A 0 μs, the initial pulse of electrons from the photoionization pulse can be seen. The low intensity well between the photoionization pulse and the second peak is the plasma expansion where no electrons escape, as illustrated in Fig. 8. The second, broad peak is when the electrons begin to escape again, and can be explained by Fig. 9. After all the electrons escape, the plasma has dissipated and there are no electrons left to detect. At approximately 120 μs, the field

ionization pulse is turned on and electrons from recombined Rydberg atoms start to be detected.

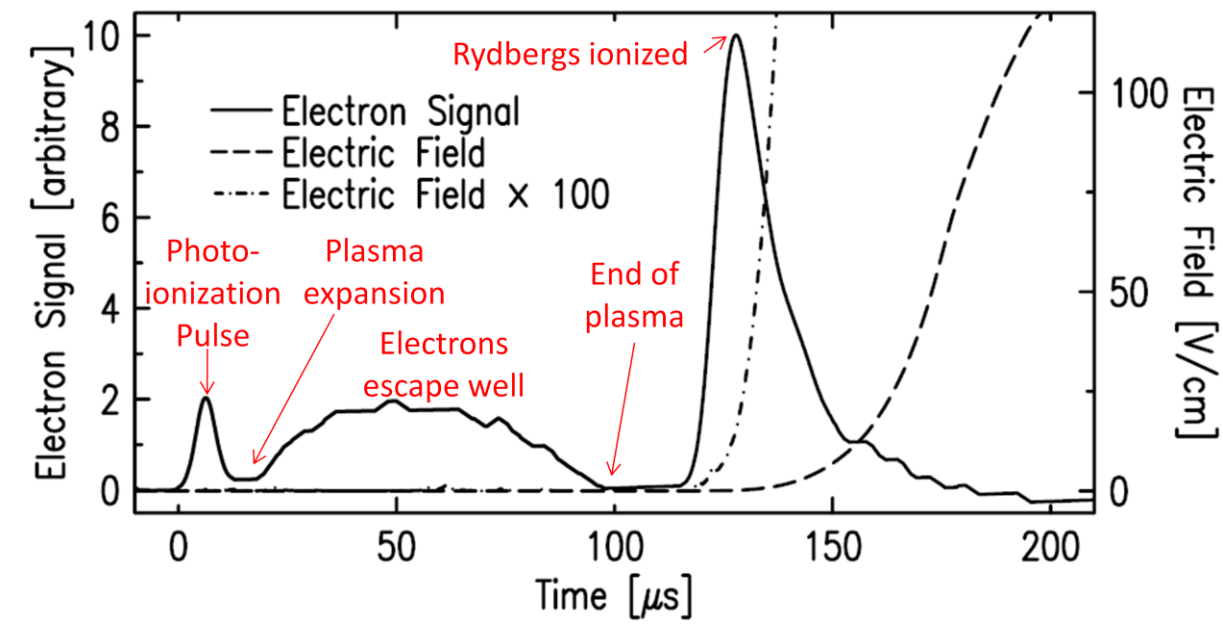

Figure 11: A schematic of the typical evolution of an ultracold plasma [4].

While the trap and repump laser function continuously, the application of the field ionization pulse is synchronized to the photoionization laser pulse. A digital delay generator (Stanford Research Systems DDG 535) connected to both makes this correlation possible. It also allows the variation of the size of the delay between the laser pulse and the application of the field ionization pulse. The delay generator is also responsible for the triggering of the digital oscilloscope used to acquire the electron signal, so it displays the repeating evolution of the plasma for one laser pulse cycle. The distribution of signals (like the one seen in Fig. 11) is known as a "Time of Flight" (TOF) spectrum. Since the time taken for the electrons to travel from the plasma to the MCP is negligible, the size of the signal at each flight time after the laser

pulse is roughly proportional to the number of electrons escaping from the plasma at that instant.

Chapter 4: Results

4.1 Electron Temperature

It has been assumed that any energy imparted to an electron during the plasma-forming ionization process in excess of the ionization potential would become the kinetic energy of that electron. This can be easily shown by considering the momentum of the ion and electron after the ionization process. The momentum of the ionizing photon is negligible, so the ion and electron have opposite but equal momentum vectors. The total energy after photoionization is therefore *E*, where

$$E = \frac{1}{2} m_+ {v_+}^2 + \frac{1}{2} m_e {v_e}^2 = \frac{{p_+}^2}{2m_+} + \frac{{p_e}^2}{2m_e} = \frac{{p_e}^2}{2m_+} + \frac{{p_e}^2}{2m_e}$$

Here, *E* is equal to the photon energy in surplus of the ionization potential, and *m, v,* and *p* are the mass, velocity, and momentum corresponding to either the electron (*e*) or the ion (*+*). Due to the fact that $m_e << m_+$, the ionic kinetic energy term is very small and can be neglected compared to the kinetic energy of the electron.

The amount of energy imparted to the atom during the ionization process corresponds to the wavelength of the photoionization laser according to the equation

$$E = \frac{hc}{\lambda} = h\nu$$

where λ is the wavelength, v is the frequency, h is Planck's constant, and c is the speed of light.

The initial temperature of the electron can be calculated from its kinetic energy

$$E = k_B T_e$$

where E is the kinetic energy of the electron, T_e is the electron's temperature, and k_B is Boltzmann's constant.

The electron's kinetic energy may be easily found by considering the energies involved in the transition and ionization processes.

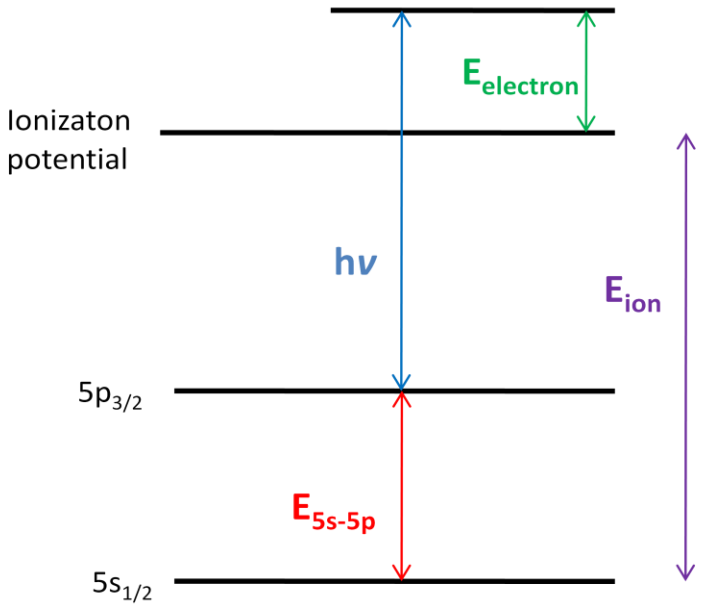

Figure 12: The relationships between the various amounts of energy involved in the rubidium ionization process. *hv* is the energy imparted by the photoionization laser, $E_{5s\text{-}5p}$ is the energy required by the $5s_{1/2} - 5p_{3/2}$ transition, E_{ion} is the amount of energy needed to ionize the atom, and $E_{electron}$ is the kinetic energy possessed by the electron.

It can be clearly seen from Fig. 12 that

$$k_B T_e = hv + E_{5s-5p} - E_{ion}$$

where $E_{5s\text{-}5p}$ is the energy of the $5s_{1/2} - 5p_{3/2}$ transition, hν is the energy imparted by the photoionization laser photon, T_e is the initial temperature of the electron, and E_{ion} is the energy needed to ionize the atom. All of these quantities, with the exception of T_e , are very precisely known.

As a result, by varying the wavelength (and thus the energy) of the photoionization laser, the electron temperature of the resulting plasma can be chosen to a very high degree of accuracy. The photoionization laser wavelength was varied to produce electron temperatures of 10 K, 100 K, and 300 K. Fig. 13 shows a plot of the electrons detected vs. time for these three temperatures. It is important to note that this plot is an inverse of the actual electron intensities measured (i.e. it is upside-down).

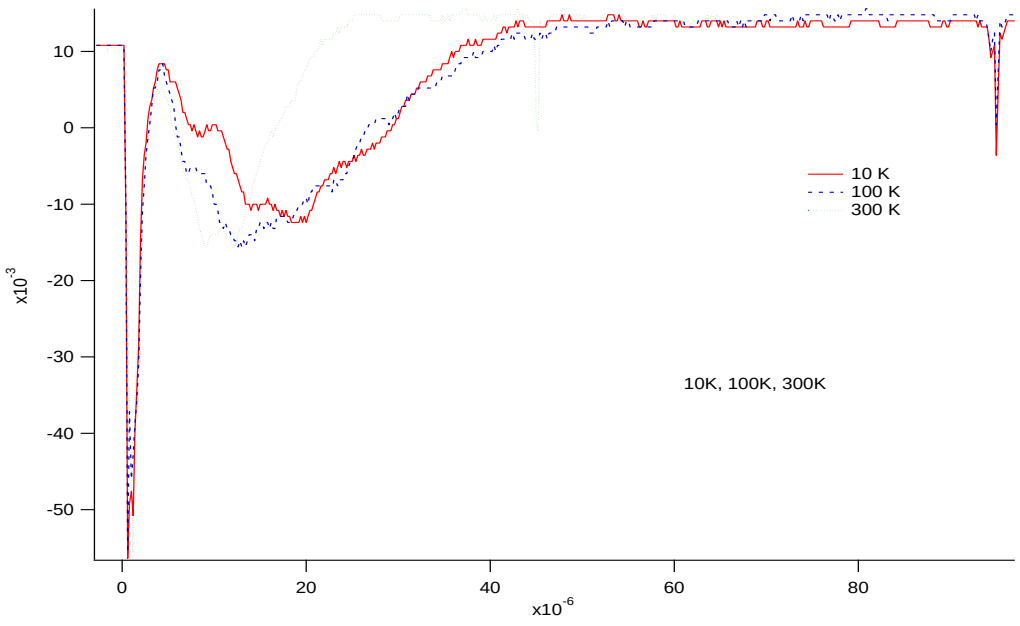

Figure 13: The graph of electron intensity vs. time of detection with varying electron temperatures. Three temperatures were observed; 10 K, 100 K, 300 K.

This graph shows the trend that was predicted. Presumably, the higher the temperature, the higher the kinetic energy of the electrons, and thus the more quickly the plasma dissipates. The graph shows the plasmas with the higher electron temperatures evolving sooner than those with lower temperatures.

Fig. 14 shows the distribution of the Rydberg atoms formed by three-body recombination for the three temperatures. The field ionization pulse that allows the observation of the Rydbergs was set to occur after the plasma naturally dissipated away. The distribution peaks are the small ones just before the 2 μs mark on the x-axis. The larger peaks that occur afterwards are secondary effects due to the ions formed by the field ionization pulse colliding with the sides of the chamber, releasing electrons that are then detected. It is interesting to note that the distribution does not appear to be affected by the temperature, since all the peaks are in the same place. Once again, the electron intensities are inverted, causing the graph to appear upside-down. The red dotted line in Fig. 14 shows the applied field ionization pulse. The time scale of the plasma evolution is on the order of tens of microseconds, and does not correspond to the markings on the x-axis.

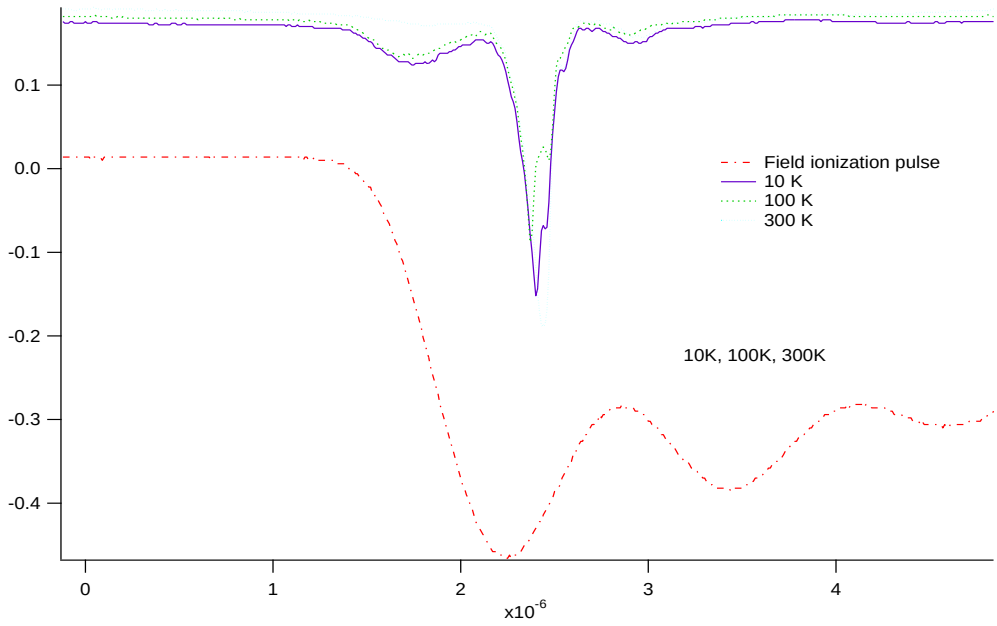

Figure 14: The graph of Rydberg electron intensity vs. time of detection with varying plasma electron temperatures. The temperatures observed were 10 K, 100 K, and 300 K. The red dotted line corresponds to the strength of the field ionization pulse.

4.2 Photoionization Laser Power

The power of the photoionization laser used to ionize the atoms corresponds to the number of rubidium atoms ionized. The greater the number of rubidium atoms ionized, the more strongly bound the plasma is because the average electron-ion distance is shorter. This increases the plasma density. It would be expected that a higher plasma density would cause

the plasma to evolve faster. This is because the more ions there are in the plasma, the higher the repulsive Coulomb forces will be, and the more swiftly the plasma will expand. This means that the electrons will escape the potential well sooner, and are detected sooner.

Three different photoionization laser powers were observed; 2.7 mW, 1 mW and 0.3 mW. The results followed what was expected. The higher the power, the sooner the electrons were observed. It is also interesting to look at the intensities of the peaks. More electrons were observed for the higher powers. This makes sense, since the number of rubidium atoms ionized (and thus the number of electrons freed) is dependent on the power of the photoionization laser.

Like the plasma and Rydberg graphs from the electron temperature section, the graphs displayed in Figs. 15 and 16 are inverted.

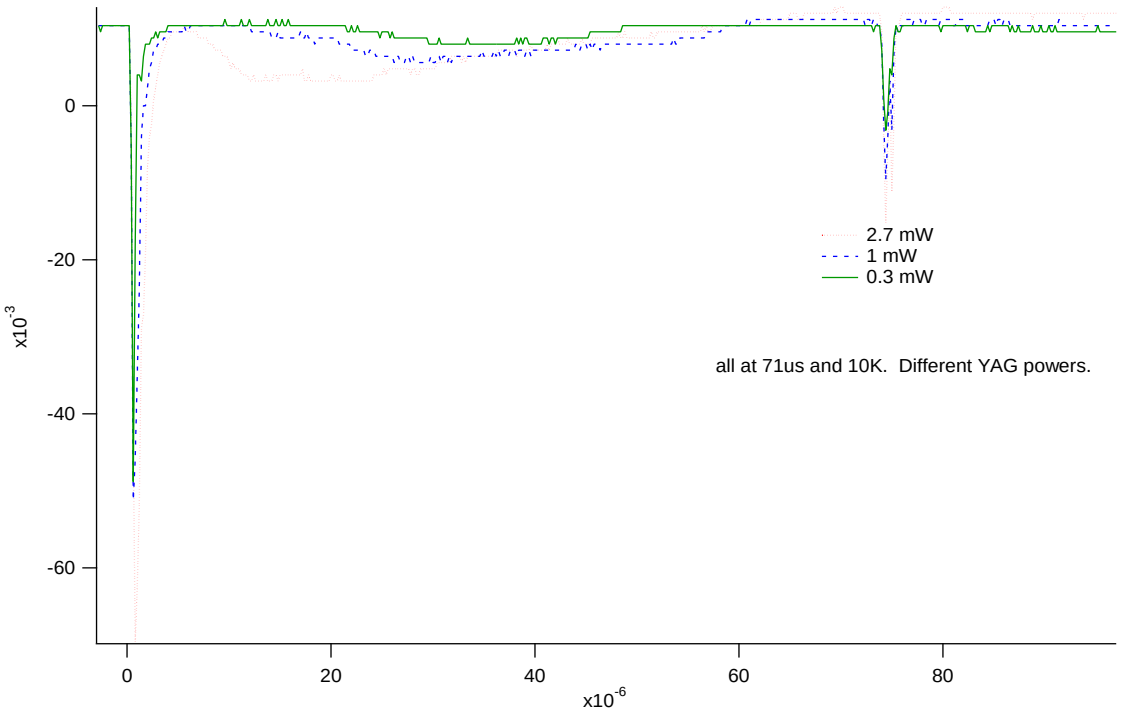

Figure 15: The graph of electron intensities vs. time of detection with varying photoionization laser powers. The powers investigated were 2.7 mW, 1 mW, and 0.3 mW.

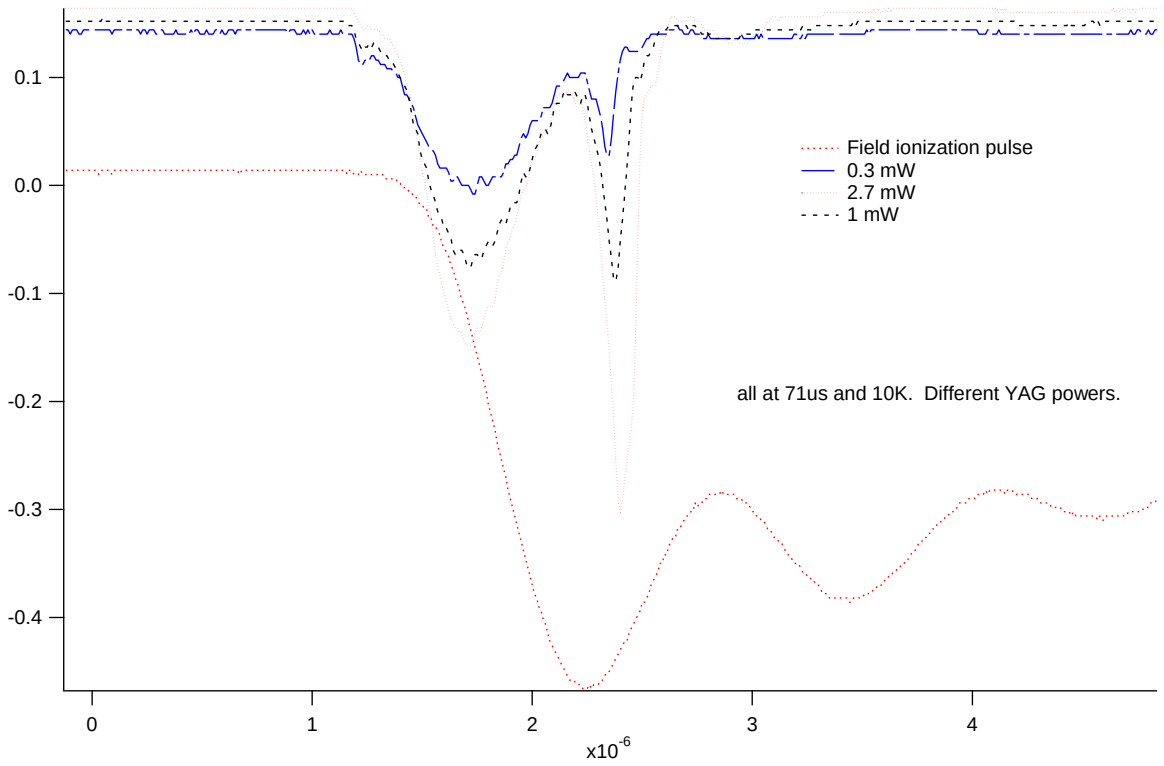

Figure 16: The graph of Rydberg electron intensity vs. time of detection with varying photoionization laser powers. The powers observed were 2.7 mW, 1.0 mW, and 0.3 mW. The red dotted line corresponds to the strength of the field ionization pulse.

4.3 Photoionization Laser Delays

The effects of a delay between the laser and the field ionization pulse were investigated. A varying delay was programmed into the timing system, setting the time between the photoionization laser pulse and the field ionization pulse to a chosen value. The distribution of the Rydberg atoms formed by recombination in the plasma was observed for different delays to test if different Rydberg state distributions formed at different times after the plasma's end.

Delays of 61 µs, 71 µs, 91µs, and 101 µs were investigated. It can be seen from Fig. 17 that the length of the delay had no effect on the distribution of Rydberg atoms formed. The large oscillations that occur before the Rydberg electrons are detected for the 61 µs trial are due to remaining plasma electrons getting blown toward the detector by the beginnings of the field ionization pulse.

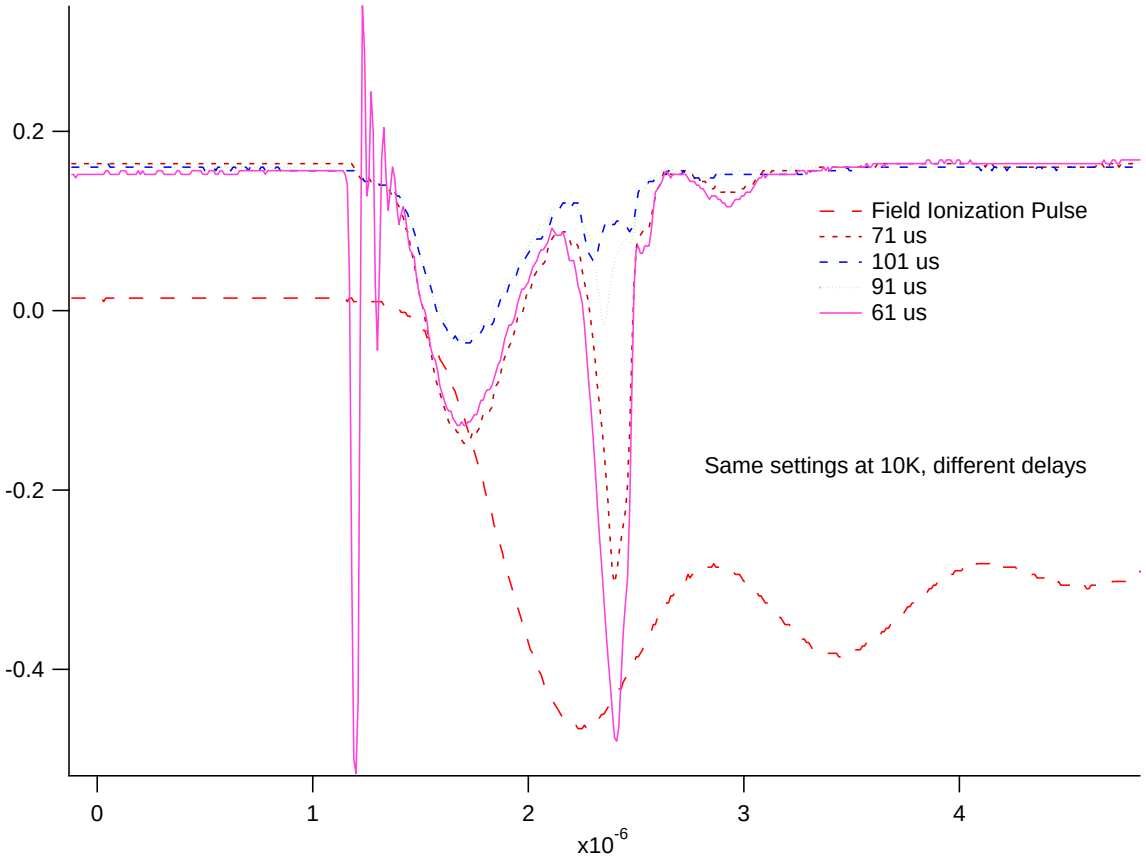

Figure 17: The graph of Rydberg electron intensity vs. time of detection with varying field ionization pulse delays. The temperatures observed were 10 K, 100 K, and 300 K. The red dotted line corresponds to the strength of the field ionization pulse. The large oscillations on the 61 µs plot are due to remaining plasma electrons being detected.

Chapter 5: Conclusion

In this thesis, three aspects of the ultracold plasma formation process were observed and measured, the first of which was electron temperature. By varying the wavelength of the photoionization laser, plasmas with different electron temperatures were created. The evolutions of these plasmas were observed through the detection of the escaped electrons. The results matched the predictions in that the higher the electron temperature, the faster the evolution of the plasma. In addition, the Rydberg atoms formed by recombination during the plasma evolution were examined. Interestingly, it was found that the electron temperature had no effect on the distribution of Rydberg states that were formed.

Also studied was the effect of the power of the photoionization laser on the plasma evolution. The photoionization laser power dictated the number of rubidium atoms that were ionized. Once again, the results corresponded to the predictions. Because more rubidium atoms were ionized, the plasma was denser and thus evolved more quickly. It is important to note, however, that it was found that this had no effect on the types of Rydberg atoms formed through recombination.

Lastly, the delay between the photoionization laser pulse and the field ionization pulse was varied. The plasma was allowed to naturally dissipate before the application of the field ionization pulse. The distribution of Rydberg states was observed to see if different Rydberg

state distributions formed at different times after the evolution of the plasma was complete. It was found that the amount of delay had no effect on the types of Rydberg atoms observed.

In the future, we would like to observe the effects of prematurely quenching the plasma before it has finished evolving. This would make it possible to determine whether different types of Rydberg atoms formed at different times in the plasma evolution. The experiment could be accomplished by applying a low electric field that dissipated the plasma before initiating the field ionization pulse to observe the Rydberg atoms.

References

1. T.C. Killian, S. Kulin, S.D. Bergeson, L.A. Orozco, C. Orzel, and S.L. Rolston. *Creation of an Ultracold Neutral Plasma*. Phys. Rev. Lett. 83, 4776 (1999).
2. S. Kulin, T.C. Killian, S.D. Bergeson, and S.L. Rolston. *Plasma Oscillations and Expansion of an Ultracold Neutral Plasma*. Phys. Rev. Lett. 85, 318 (2000).
3. J.L. Roberts *et al. Electron Temperature of Ultracold Plasmas.* Phys. Rev. Lett. 92, 253003 (2005).
4. T.C. Killian, M.J. Lim, S. Kulin, R. Dumke, S.D. Bergeson, and S.L. Rolston. *Formation of Rydberg Atoms in an Expanding Ultracold Neutral Plasma.* Phys. Rev. Lett. 86, 3759 (2001).
5. R.S. Fletcher, X.L. Zhang, and S.L. Rolston. *Using Three-Body Recombination to Extract Electron Temperatures of Ultracold Plasmas.* Phys. Rev. Lett. 99, 145001 (2007).
6. K.B. MacAdam, A. Steinbach, and C. Weiman. *A narrow-band tunable diode laser system with grating feedback, and a saturated absorption spectrometer for Cs and Rb.* Am. J. Phys. 60, 1098 (1992).
7. J. Ye, S. Swartz, P. Jungner, and J. Hall. *Hyperfine structure and absolute frequency of the ^{87}Rb $5P_{3/2}$ state.* Optics Letters 21, 1280 (1996).
8. S. A. Lee, J. Helmcke, J.L. Hall, and B.P. Stoicheff. *Doppler-free two-photon transitions to Rydberg levels: convenient, useful, and precise reference wavelengths for dye lasers.* Optics Letters 3, 141 (1978).
9. C. Wieman and G. Flowers. *Inexpensive laser cooling and trapping experiment for undergraduate laboratories*. Am. J. Phys. 63, 317 (1995).
10. Bill Whitledge. *Diode Lasers for Use in Experiments on Cold Rydberg Atoms*, Physics Honors Thesis, 2008.